An investigation on the fatigue performance of cracked steel plates reinforced with FRP and stop hole

Liu, Zhiping; Li, Zongchen; Huang, Chuanhai; Jiang, Xiaoli

DOI
10.1080/15376494.2021.1907005

Publication date
2021

Document Version
Final published version

Published in
Mechanics of Advanced Materials and Structures

Mechanics of Advanced Materials and Structures

ISSN: (Print) (Online) Journal homepage: https://www.tandfonline.com/loi/umcm20

An investigation on the fatigue performance of cracked steel plates reinforced with FRP and stop hole

Zhiping Liu, Zongchen Li, Chuanhai Huang & Xiaoli Jiang

To cite this article: Zhiping Liu, Zongchen Li, Chuanhai Huang & Xiaoli Jiang (2022) An investigation on the fatigue performance of cracked steel plates reinforced with FRP and stop hole, Mechanics of Advanced Materials and Structures, 29:25, 3646-3657, DOI: 10.1080/15376494.2021.1907005

To link to this article: https://doi.org/10.1080/15376494.2021.1907005

Published online: 07 Apr 2021.

MECHANICS OF ADVANCED MATERIALS AND STRUCTURES
2022, VOL. 29, NO. 25, 3646–3657
https://doi.org/10.1080/15376494.2021.1907005

Taylor & Francis
Taylor & Francis Group

ORIGINAL ARTICLE

An investigation on the fatigue performance of cracked steel plates reinforced with FRP and stop hole

Zhiping Liu[a,b], Zongchen Li[c,d], Chuanhai Huang[a], and Xiaoli Jiang[d]

[a]School of Logistics, Wuhan University of Technology, China; [b]Port Logistics Technology and Equipment Engineering Research Centre of Ministry of Education, Wuhan, China; [c]Mechanical Systems Engineering, EMPA-Swiss Federal Laboratories for Materials Science and Technology, Duebendorf, Switzerland; [d]Department of Maritime and Transport Technology, Delft University of Technology, Delft, The Netherlands;

ABSTRACT

In this paper, we implement the combined method of drilling stop hole and FRP reinforcement to repair cracked steel plates subjected to cyclic tension. The crack initiation and growth are experimentally investigated. The stress distribution at the stop hole and the residual fatigue life are evaluated by the FEM. The effects on prolonging residual fatigue life are analyzed. The results show that the effectiveness of only using the stop hole is limited, while the combined method has dramatically prolonged the residual fatigue life. The effect mainly owes to the increasing of the crack initiation life from the stop hole.

ARTICLE HISTORY
Received 7 January 2021
Accepted 18 March 2021

KEYWORDS
Crack initiation; drilling stop hole; fatigue life; fatigue performance; FRP reinforcement

1. Introduction

Fatigue crack is a common defect of steel structures after long-term effects of varying loads and various environmental factors [1]. If not timely and effectively treated, it might eventually lead to structural fatigue failure. The emergence of repair and reinforcement technology provides a new way of solving this problem. Compared to replacing damaged structural parts, repair and reinforcement techniques have great advantages both in terms of time and cost [2, 3].

The use of a crack stop hole at the crack tip is one of the most commonly used techniques of temporary control. In past a few decades, engineering application of crack stop hole has been studied by many scholars [4, 5]. The results showed that a reasonable design of the shape, size and position of the crack stop hole can effectively decrease crack growth rate and increase the residual fatigue life. However, when the crack stop hole is processed at the fatigue crack tip, the mechanical strength of the original structure is weakened and a new fatigue-prone area is created. More importantly, when the crack is initiated from the edge of the crack stop, the rate of expansion of the new crack does not change as a result of the presence of the stop hole [6].

As a composite material, fiber reinforced polymer (FRP) material has a high strength-to-weight ratio, good corrosion resistance as well as fatigue performance, and can be processed into almost any desired shape. In the past few years, the reports on the influence of structural defect size [7, 8], properties of adhesives [9, 10] and FRP bonding method [11–13] on reinforcement effect indicated the great potential of using FRP to reinforce structures. However, this method does not eliminate structural damage, and the crack propagates directly on the original defect after reinforcement.

The crack stop hole alleviates the stress concentration at the crack tip to prevent or postpone the extension of the crack [14] while the FRP reinforcement method realizes the same function by compensating for the mechanical strength caused by the structural loss. Reddy et al. [15] showed that the combination of the stop hole and the FRP reinforcement can synergize the advantages of the two methods. Alemdar et al. [16] analyzed the effects of different reinforcement parameters on crack growth rate, but did not consider the initiation stage of new cracks. Overall, the existing literatures mainly focused on the crack growth rate after reinforcement; while, the crack initiation and propagation after reinforcement has not been studied. Studying the fatigue performance of the structure repaired by the two methods simultaneously can improve the application confidence of the FRP reinforcement technology on one hand, and provide some guidance for practical engineering applications on the other hand.

Given that, in this paper, the combined two methods are implemented to repair the cracked steel plates subjected to cyclic tension. The stop holes are made in the cracked steel plates at different stages with different crack lengths. Then the FRP reinforcement is applied on the specimens, either on one side or on both sides. In Section 2, an experimental study is conducted on the specimens repaired only by stop hole, or by both methods on different crack lengths. In Section 3, the finite element

CONTACT Zongchen Li zongchen.li@empa.ch Mechanical Systems Engineering, EMPA-Swiss Federal Laboratories for Materials Science and Technology, Duebendorf, Switzerland

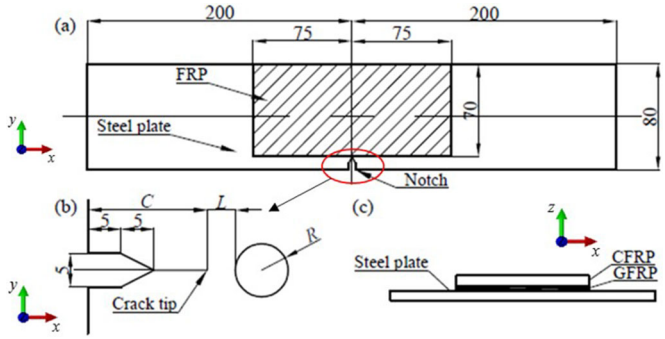

Figure 1 Specimen geometry: a) sample size and CFRP paste area: (b) fatigue crack and crack stop-hole size: (c) cross-section view of the specimen.

(FE) analysis is performed to analyze the stress distribution at the stop hole and the residual fatigue life. Note that besides the FE method, which requires very fine meshes around the crack front area, in recent decades, robust meshless techniques for fracture analysis of steel structures and composite structures gained huge popularities [17–19]. While in this paper, the traditional FE method is adopted, mainly considering the need of evaluating both the crack initiation and propagation. Section 4 discusses and analyses the experimental and numerical results. Finally, the conclusions are drawn in Section 5.

2. Experimental study

2.1. Material properties

The cracked steel plate specimens are repaired only by the stop hole, or with the FRP as well (see in Figure 1a), containing four different materials: the steel substrate, Glass-FRP (GFRP), Carbon-FRP (CFRP), and adhesive. Stainless steel of Q235B conforming to GB/T 700-2006 code [20], which has a yield stress of 235 MPa, and tensile stress of 400 MPa, has been used as the steel substrate. The elastic modulus and passion ratio of the steel is 2.10×10^6 MPa and 0.274, respectively. The E-glass fiber weave material was applied as the GFRP laminate, while T700 series unidirectional carbon fiber was used as the CFRP material. Their material properties are listed in Tables 1 and 2, respectively. The adhesive adopted the resin epoxy conforming to the code GB/T 2567-2008 [21], which material properties are listed in Table 3. Note the material properties are all provided by each corresponding manufacturer.

2.2. Specimen manufacturing

The specimen manufacturing contains four main steps: notch manufacturing, pre-cracking, stop hole making, and the FRP reinforcement. First, a triangular shaped notch was manufactured for the sake of generating fatigue cracks. The detail and the size of the notch is shown in Figure 1b. Then the pre-cracking procedure was conducted to initiated fatigue cracks from the notches [22]. The importance of the pre-cracking is to provide a sharpened fatigue crack of adequate size and straightness which ensures that: 1) the effect of the machined starter notch is removed from the specimen Stress Intensity Factor (SIF)-calibration, and 2) the effects on subsequent crack growth rate data caused by changing

Table 1. Material properties of GFRP.

E_1 (Pa)	E_2 (Pa)	T (Pa)	G_{13} (Pa)	G_{23} (Pa)	Nu_{12}
72×10^9	72×10^9	1.1×10^9	4.7×10^9	3.5×10^9	0.33

Note: E is the tensile elastic modulus, T is the tensile strength, G_{ij} is the shear modulus, and Nu is the Poisson's ratio.

Table 2. Material properties of the Toray 700S CFRP material.

E_1 (Pa)	E_2 (Pa)	T_1 (Pa)	G_{13} (Pa)	G_{23} (Pa)	Nu_{12}
230×10^9	25×10^9	4.9×10^9	5.5×10^9	3.0×10^9	0.33

Note: T_1 is the tensile strength along the main direction.

Table 3. Material properties of resin epoxy.

E (Pa)	T (Pa)	G (Pa)	Nu
2.8×10^9	30×10^6	1.05×10^9	0.35

crack front shape or pre-crack load history are eliminated. In addition, the basic regulation is the crack growth rate during the pre-cracking procedure should be below 10^{-8} m/cycle [22], and ASTM E2899 suggested the two-step pre-cracking procedure that the SIF at the first 50% should be smaller than 30MPa $\cdot m^{1/2}$, and at the second 50% smaller than 25MPa $\cdot m^{1/2}$ [23]. Hence, in this experimental investigation, we conducted two stages of the pre-cracking on the fatigue machine: the first stage adopted 80% yield stress as the load amplitude of the constant amplitude sinusoidal cyclic loading, while the second stage adopted 40% yield stress, respectively. Note that both of the two stages were under the load ratio equals to 0.1. During each stage, tensile fatigue load was applied on the specimens. Eventually, the crack initiated from the notch and propagated more than 1.0 mm. Then the size of each fatigue crack after the pre-cracking procedure was regarded as the initial crack size.

Afterwards, the cracked steel plates were repaired by drilling stop holes, following the CECS 77:96 standard [24]. The stop hole is manufactured along the extension line of the fatigue crack. The distance L between the crack tip and the stop hole, as well as the diameter of the stop hole R, are 4 mm, as shown in Figure 1b.

Thereafter, the specimens were reinforced with the FRP laminates on either one or both sides of the steel plates by hand lay-up technique. The FRP laminates were bonded in the middle of the specimen, as shown in Figure 1a. In light of the galvanic corrosion between CFRP laminates and steel substrate, one layer of GFRP laminate was adopted as the first layer of the FRP reinforcement, as shown in Figure 1c. The reinforcement procedure contained the surface preparation, cleaning, composite laminates pasting. Each two adjacent layers were bonded together by the adhesive. Finally, the FRP laminates were compressed by a large mass in order to squeeze redundant resin epoxy and eliminate the bubbles in the interlaminations, as well as to let each laminate bonded tightly. Then the specimens were placed at room temperature for solidification of one week, in order to achieve the optimum bond condition.

2.3. Specimen configurations

The steel plate is 400 mm long, 80 mm wide, and 8.0 mm thick. The width of each GFRP and CFRP laminate equals to 70 mm, and the length of each FRP laminate is 150 mm. The thickness of

Table 4. Specimens' configurations and FRP reinforcement details.

Group	Specimen	a_0 (mm)	Repair method	FRP reinforcement method	No. of CFRP layers
H1	C16-H-1	16.0	Stop hole	/	/
	C16-H-2	16.0	Stop hole	/	/
H2	C22-H-1	22.0	Stop hole	/	/
	C22-H-2	22.0	Stop hole	/	/
H3	C28-H-1	28.0	Stop hole	/	/
	C28-H-2	28.0	Stop hole	/	/
HS1	C16-HS-1	16.0	Stop hole and FRP reinforcement	Single side	4
	C16-HS-2	16.0	Stop hole and FRP reinforcement	Single side	4
HS2	C22-HS-1	22.0	Stop hole and FRP reinforcement	Single side	4
	C22-HS-2	22.0	Stop hole and FRP reinforcement	Single side	4
HS3	C28-HS-1	28.0	Stop hole and FRP reinforcement	Single side	4
	C28-HS-2	28.0	Stop hole and FRP reinforcement	Single side	4
HD1	C28-HD-1	28.0	Stop hole and FRP reinforcement	Double side	4
	C28-HD-2	28.0	Stop hole and FRP reinforcement	Double side	4×2

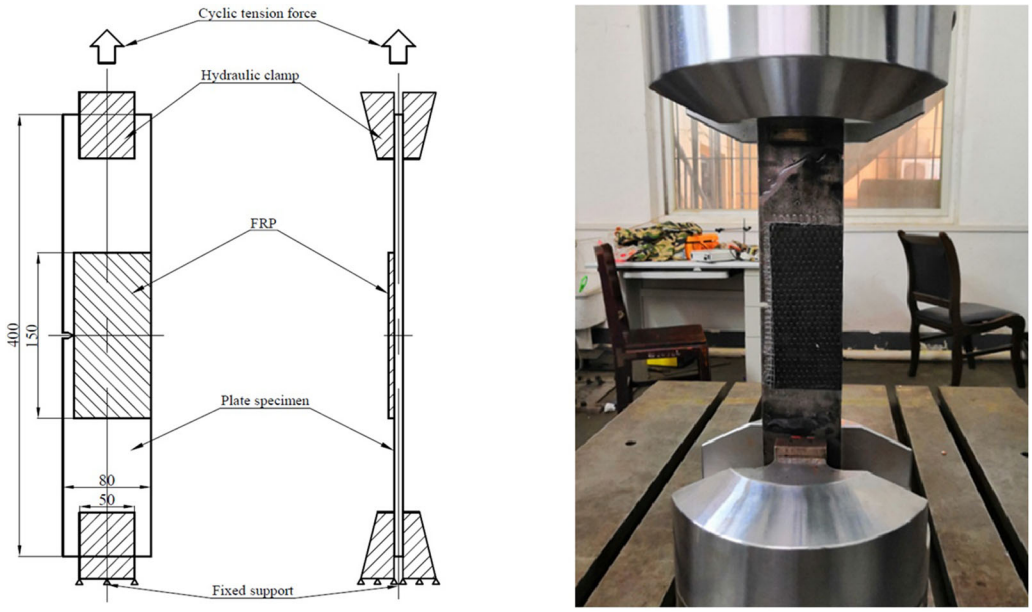

Figure 2. Specimen installation: a) the schematic; b) the actual specimen installation.

each layer of GFRP and CFRP laminate are 0.35 mm. Each FRP reinforced specimen applies one layer of GFRP as the first layer, and several layers of CFRP laminate on top of that, as shown in Figure 1c. The configuration of the specimens and reinforcement details are listed in Table 4. In total, seven groups of 14 specimens were prepared. Each group contains two repetitive specimens. Group H1, H2, and H3 are three groups with different initial crack sizes repaired by stop holes. Groups HS1, HS2, and HS3 are the three corresponding groups to the previous groups while adopts both the stop hole and the single-side FRP reinforcement method. Group HD1 is the group corresponding to group HS3 while applies the FRP reinforcement on both sides. The name of the specimens in Table 4 represents the crack size, reinforcement method and its repetitive number. Take 'C16-HS-1' as an example, 'C16' means crack length is 16 mm, 'HS' represents the stop hole and the single-side FRP reinforcement, the number '1' stands for the No. of the repetitive specimen.

2.4. Test set-up

The fatigue tests were conducted under constant amplitude sinusoidal cyclic loading, generated by MTS Hydraulic Actuator, which has a capacity of 250 kN. The schematic of test setup and the real test setup is shown in Figure 2. Two edges of each tensile specimen were clamped by a pair of hydraulic clamps, positioned horizontally on the fatigue machine. The load was applied in tension condition to ensure a pure tension statue for the plate specimen. Note that the fatigue test follows the code of ASTM E647 [22].

All the fatigue tests were conducted at room temperature and air environment under load control condition. The loading frequency was set as 15.0 Hz. The load ratio maintained 0.1 for the crack growth process of all tests. The crack growth process was recorded by Beach Marking technique by means of changing the load ratio from 0.1 after every 8,000 cycles to 0.55 for 4,000 cycles, as described in Figure 3. Each test ended automatically once the tensile specimen fractured and trigger the displacement limiter of the fatigue machine.

2.5. Test phenomena

When only using the stop hole to repair the cracked steel plate of 'C16-H-1' which has a 16.0 mm crack length, three

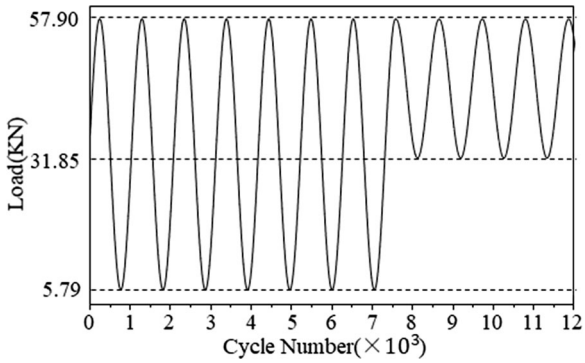

Figure 3. The load spectrum and beach mark generating procedure.

regions of crack propagation were clearly observed from the specimen cross section: the crack initiation zone (A), the stable cracking area (B) and the fast facture zone (C), as shown in Figure 4a. While for the specimen of 'C28-H-1' which crack length is already 28.0 mm, the crack grew rapidly to fracture with no beach marks recorded on the cross-section, as shown in Figure 4b.

In light of the specimens of which used the two repair method, i.e., drilling stop hole and the FRP reinforcement, three failure modes were observed for the single-side FRP reinforced specimens after each test: the interfacial failure, cohesion failure, and the FRP rupture. Figure 5a shows the rupture of both the GFRP and CFRP laminates, while some of the FRP laminates were stick on the steel substrate, the other FRP filaments were debonded as a whole from the steel substrate. Figure 5b shows the FRP laminates entirely debonded from the steel substrate. Meanwhile, the adhesive partly remained on the steel substrate.

3. Finite element analysis

The experimental study in Section 2 focuses on the crack initiation and crack growth of the steel plates repaired by the stop hole and the FRP laminates. In this section, we develop a three-dimensional FE model for analyzing the stress distribute at the stop hole, evaluating the crack initiation life and crack propagation.

3.1. Modeling strategy

The FE modeling and analysis are conducted in the commercial software ABAQUS 2019. FE models of the cracked steel plate models repaired only by stop hole, or with the FRP reinforcement as well, are shown in Figure 6. The materials, dimensions, and load condition of the FE models are identical to the experimental specimens. Conforming to the test specimens, the thickness of each layer is 0.35 mm. The thickness of the adhesive is 0.1 mm. Then the crack path is assigned at the middle of the model, along the width direction, as shown in Figure 6a. Fixed support is assigned at one edge face of the model, while tensile force is assigned at the other edge face of the FE model, as shown in Figure 6b. The crack tip and the stop hole are modeled and meshed as concentric cycles, as indicated in Figure 6c.

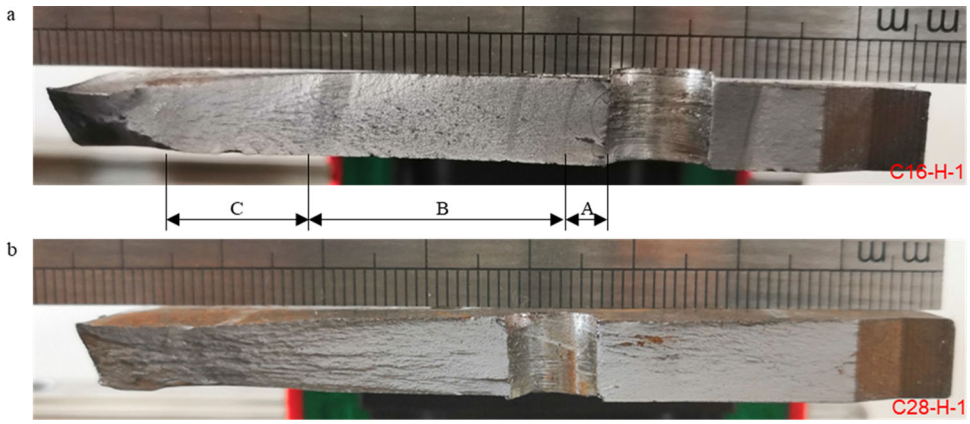

Figure 4. Cross-section view along the crack surface: a) specimen C16-H-1; b) specimen C28-H-1.

Figure 5. Failure modes of single-side reinforcement: a) FRP rupture; b) interfacial debonding and cohesion failure.

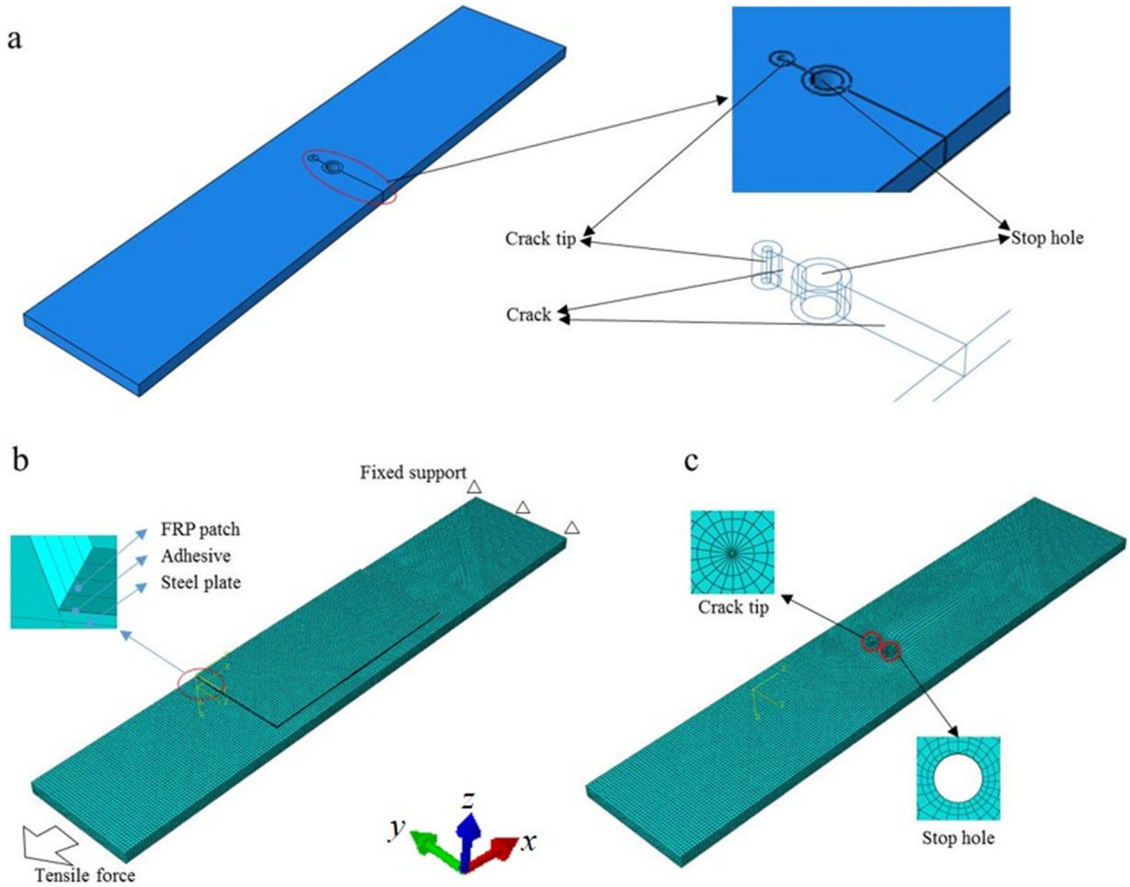

Figure 6. The FE model and global meshing condition of the cracked steel plate reinforced with FRP.

The modeling strategy (e.g., element type, meshing method, element size) has been discussed through the sensitivity analysis in previous studies to verify the FE model [25]. The steel pipe excludes the crack front region, as well as the composite laminates, apply the 20-node quadratic brick element C3D20R, while the crack front area adopts the 15-node quadratic triangular prism element C3D15. The interface between the steel substrate and the FRP laminates is modeled through the Cohesive Zone Modeling (CZM) using the 8-node three-dimensional cohesive element COH3D8, which is based on the bi-linear traction–separation law. The constraints of FRP–adhesive–steel interactions are set as tie. The areas excluded the cracked area was meshed using hexahedral element by the sweeping method, while the cracked area around the crack tip is meshed using the wedge-shaped elements. The element size is set as 2.0 mm in order to provide robust and accurate results. Finally, the SIF of the crack is evaluated through the contour integral method.

The adhesive layer adopts the resin epoxy, which mechanical properties are listed in Table 3. In addition, a traction–separation behavior, as shown in Figure 7, is integrated into the adhesive layer to simulate the interfacial bond condition, using the CZM. The properties of the traction–separation model is listed in Table 5. The values are calculated by the method in Ref. [26], as indicated from Equations (1) to (5). G_c is evaluated as

$$G_c = 31\left(\frac{T}{G}\right)^{0.56} t_a^{0.27}. \quad (1)$$

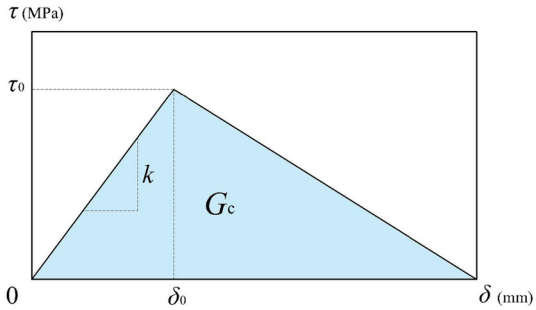

Figure 7. The bi-linear traction–separation law.

Table 5. The properties of the traction–separation model.

τ_0 (MPa)	δ_0 (mm)	δ (mm)	k (MPa/mm)	G_c (N/mm)
18	0.00386	0.252	4663	2.268

where T is the tensile strength, as indicated in Table 3. The shear strength is estimated as

$$\tau_0 = 0.8 \cdot T, \quad (2)$$

and δ_0 is calculated as

$$\delta_0 = \frac{t_a \tau_0}{G}, \quad (3)$$

where t_a is the adhesive thickness, and G is the shear modulus of the adhesive. δ is calculated as

$$\delta = \frac{2G_c}{\tau_0}, \tag{4}$$

The slope of the ascending part is equated to the shear stiffness of the adhesive layer, which is

$$k = \frac{\tau_0}{\delta_0}; \tag{5}$$

In Table 5, τ_0 is the shear strength, δ is the displacement when interfacial failure occurs, δ_0 is the displacement corresponding to τ_0, k is the shear stiffness, G_c is the energy release rate. The interfacial stiffness starts to degrade when the value of the peeling stress exceeds τ_0. The degree of the degradation is represented by the scalar stiffness degradation variable (SDEG) from 0 to 1. The interfacial stiffness completely vanishes when the SDEG reaches 1.0, representing the occurring of the debonding failure. The effect of the interfacial stiffness degradation on the SIF has been considered within the FE model. And then combining with the Paris's law, the crack growth rate is evaluated.

3.2. Crack initiation evaluation by the FE method

The crack initiation of high cycle fatigue evaluated by the FE model is based on the S–N curve theory, adopting the Basquin equation [27], which is,

$$\sigma^A N = p, \tag{6}$$

where A and p are the coefficients related to the material properties, stress ratio and the loading case. In this paper, the values of A and p is estimated by Equations (7)–(11)

$$\sigma_f = \begin{cases} q\sigma_u, & \sigma_u < 1400 \text{ MPa} \\ 1400q, & \sigma_u \geq 1400 \text{ MPa}, \end{cases} \tag{7}$$

where σ_f is the stress value when the initiation life N is infinity, which is known as the fatigue limit, q is a coefficient equals to 0.35 when under cyclic tension, σ_u is the material ultimate strength for brittle materials while is the yield strength for ductile materials [28].

Assuming the stress value is $0.9\sigma_u$ when N equals to 10^3, and the stress value increase to σ_f when N becomes 10^7, then from Equation (6), we get

$$(0.9\sigma_u)^A \cdot 10^3 = p \tag{8}$$

$$\sigma_f{}^A \cdot 10^6 = p. \tag{9}$$

Then by incorporating Equations (3) and (4), we get

$$A = \frac{3}{\lg 0.9 - \lg q} \tag{10}$$

$$p = lg^{-1}\left[\frac{6\lg 0.9 + 3(\lg\sigma_u - \lg q)}{\lg 0.9 - \lg q}\right]. \tag{11}$$

Hence the S–N curve which is appropriate for the initiation life between 10^3 and 10^6 is evaluated, where $A = 7.314$, and $p = 1.02 \times 10^{20}$.

In this subsection, the FE model simulated by ABAQUS is combined with the professional software FE-SAFE [29] for evaluating the crack initiation life, illustrated by the flowchart in Figure 8 [31]. First, the stress results are evaluated by

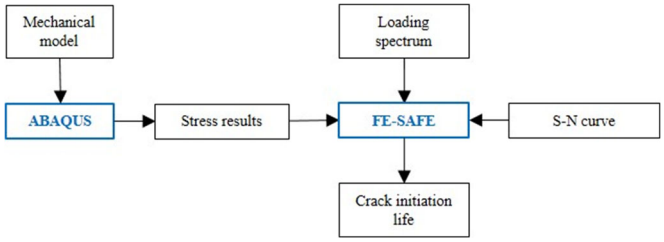

Figure 8. Flowchart of combing ABAQUS and FE-SAFE to evaluate the crack initiation life [31].

Table 6. The fatigue properties of the steel.

Coefficient	Value
Cycle strength coefficient (MPa)	999.76
Cyclic strain strengthening index	0.1992
fatigue strength exponent	–0.08
fatigue ductility exponent	–0.462
Fatigue ductility coefficient	0.1559
Fatigue strength coefficient (MPa)	630

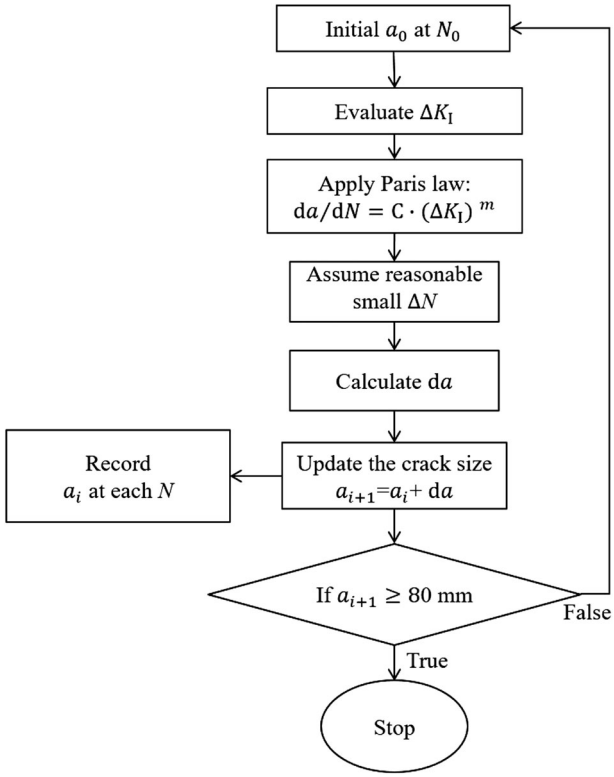

Figure 9. The procedure of evaluating the crack growth process.

ABAQUS using the structural static analysis. Then the stress data is imported into the FE-SAFE for evaluating the crack initiation life, by setting the loading spectrum, S–N curve coefficients. The fatigue properties for the evaluation in the FE-SAFE are listed in Table 6, provided by Ref. [30].

3.3. Crack propagation evaluated by the FE method

The SIF of the crack is evaluated by the FE method. Then combining the Paris' law [32], the crack growth process can be evaluated. Figure 9 shows the procedure of evaluating the crack growth process. First, the range of the SIF, which is

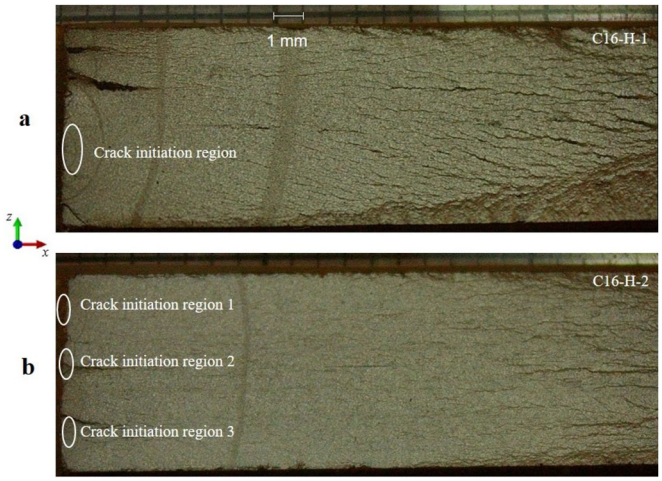

Figure 10. Partial section of the specimens repaired only by the stop hole: a) single point initiation; b) multi-point initiation.

ΔK_I, is evaluate by the FE method, based on the input crack length a and initial cyclic number N_0. Then the crack growth rate da/dN is evaluated by the Paris' law. After that, by assigning a small amount of cyclic number ΔN, the corresponding crack increment Δa is obtained. Thereafter, we get a new crack length a_i with the corresponding N_i. Repeating the process until a equals or exceeds the width of the plate, then finally we obtained the dataset of crack length-cyclic number.

4. Results and discussion

In this section, the experimental and FE results in terms of the total fatigue life, crack initiation life, crack growth process, possible failures between the FRP laminates and the steel substrate are presented and analyzed.

4.1. The location of crack initiation from the stop hole

The crack initiated from multiple regions from the stop hole of two repetitive specimens that were repaired only by the stop holes, as shown in Figure 10. It can be seen that in most cases, the cracks were initiated from the middle areas of the stop hole's surface rather than the surface of the steel plate. The crack initiated and propagated in 'C16-H-1' from one region as curve shaped (see in Figure 10a), while the cracks in 'C16-H-2' shown in Figure 10b initiated from three different regions and they finally merged into a larger crack. In general, the crack in 'C16-H-2' grew faster than the crack in 'C16-H-1', which means the multi-crack initiated from the stop hole grows faster than single-crack initiation at the early stage.

The crack initiation location on the single-side FRP reinforced specimens had an obvious difference to the specimens without FRP reinforcement, as shown in Figure 11. In all cases, the cracks initiated from the un-reinforced surface of the steel plate, due to the higher stress concentration. Then the crack propagated as a corner elliptical crack and continually propagated to a through-thickness crack. In this case, the FRP has significantly prolonged the fatigue life

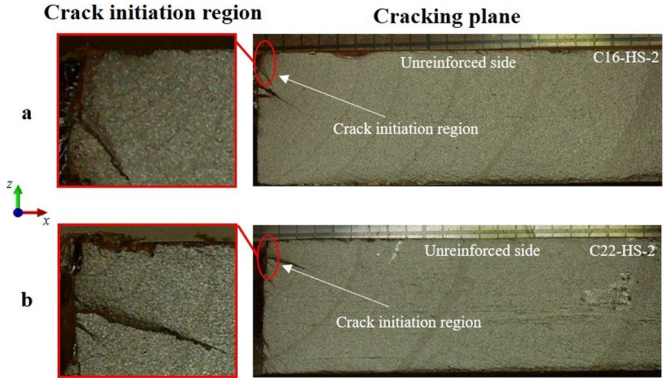

Figure 11. Partial section of a single-side FRP reinforced specimens: a) crack length 16 mm; b) crack length 22 mm.

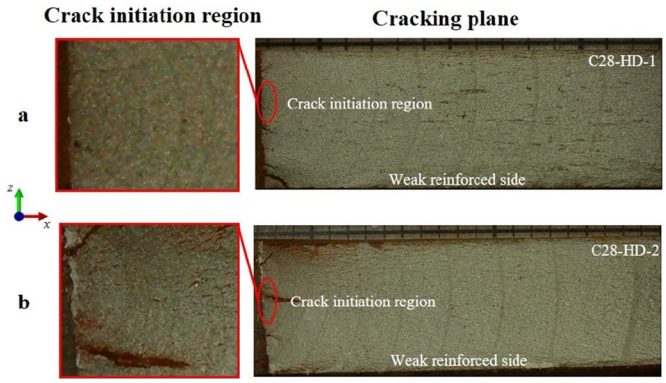

Figure 12. Partial section of double-side reinforced specimens: (a) C28-HD-1 (b) C28-HD-2.

from crack initiation till penetrating the wall thickness. Figure 11b shows that the 'C22-HS-2' with a longer crack length, grew much faster than the crack in 'C16-HS-2' (see in Figure 11a)—nine beach marks were recorded on the cross-section till penetrating the wall thickness, which represents 63,000 cycles for 'C16-HS-2', while only four beach marks for 'C22-HS-2' which represents 28,000 cycles under load ratio equals to 0.1.

When using the double-side FRP to reinforce the specimens, the cracks initiated around the middle area of the stop hole surface, as shown in Figure 12. Compare with the single-side FRP reinforcement in Figure 11, the double-side FRP has significantly prolonged the fatigue life even with a longer crack, indicated by the number of beach marks.

The FE results in Figure 13 clearly illustrate the distribution of the maximum principle stress (perpendicular to the tensile load) at the stop hole. It shows that for the model repaired only by the stop hole (Figure 13a) and the model repaired by the stop hole and the double-side FRP reinforcement (Figure 13c), the maximum stress value is located at the middle of the inner surface of the stop hole, as indicated by Figure 14. This makes the cracks initiated from the middle area of the inner surface of the stop hole, as shown in Figures 10 and 12, respectively. Note the results of the maximum principle stress in Figure 14 are extracted from the nine nodes along the black arrow inside the stop hole, indicated by Figure 13b along the black arrow. Figure 13 also shows the double-side reinforcement has significantly decreased the maximum stress value from 1584 MPa to

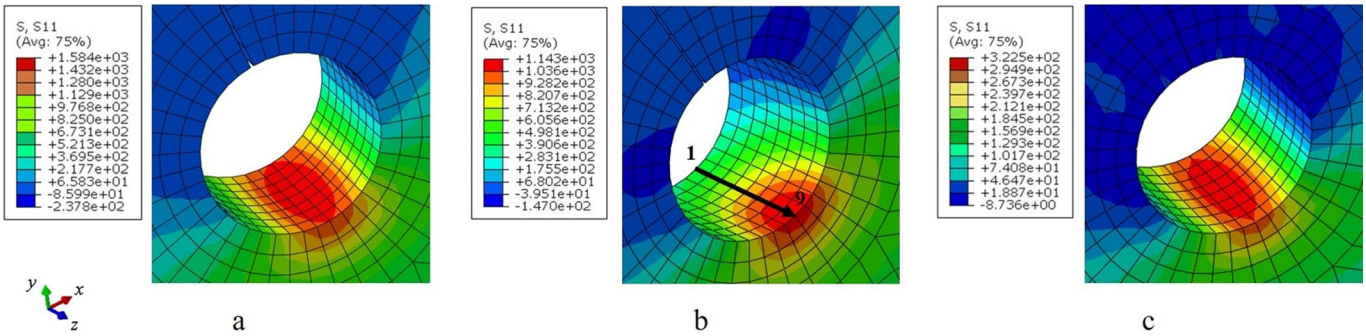

Figure 13. The illustration of the maximum principle stress at the stop hole evaluated by the FE method: a) C28-H; b) C28-HS; c) C28-HD.

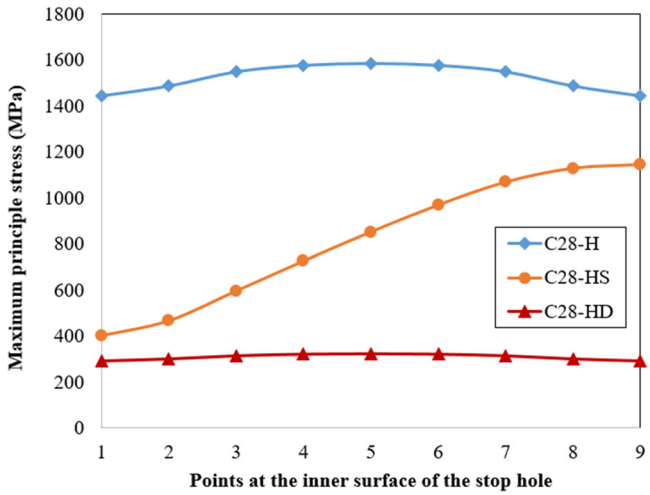

Figure 14. Maximum principle stress at the points along the inner surface of the stop hole.

323 MPa, of 79.6%, resulting in the significant increasing of the initiation life, as indicated in Table 6. For the model repaired by the stop hole and the single-side FRP reinforcement (Figure 13b), the location of the maximum stress shifts from the middle point to the surface point of the reversed side of the reinforced surface, and the value decreased to 1143 MPa, of 27.8%.

4.2. FRP-to-steel interface bond condition

The results of the bond conditions of different models when the crack reached 56 mm (10 mm propagation from the stop hole of the C28-HS and C28-HD models) are shown in Figure 15, where the number index represents the SDEG value of the contact interface. The results show that none of the SDEG value of the specimens reached 1.0, meaning that the bond between the FRP laminates and the steel substrate have not completely failed. However, the values of the SDEG that are very close to 1.0, indicating that serious stiffness degradations have already occurred seriously. The comparisons between Figure 15a and 15b, as well as Figure 15c and 15d, show the stiffness degradation of the single-side FRP reinforced models is more serious in terms of the area and the degree of the degradation. The comparisons between the Figure 15a and 15c, as well as Figure 15b and 15d shows the crack propagation from the stop hole has further aggravate the degradation around the stop hole and along the crack growth path. Overall, the crack propagation and the stop hole have induced the serious stiffness degradation at the FRP-to-steel interface, while debonding failures have not occurred.

The SDEG variation along with the increase of the applied stress, indicated by the SDEG vs. remote stress curve of C28-HS with a 10 mm crack initiated from the stop hole as an example (corresponding to Figure 15b), is shown in Figure 16. The figure shows the stiffness degradation occurs when the remote stress reaches nearly 20 MPa, and quickly increases along with the increase of the remote stress. Then the SDEG grows slower along with the remote stress, until it reaches its maximum of 0.992 with the maximum remote stress of 90.48 MPa.

4.3. Results of the fatigue life

For a cracked plate with a stop hole, its cross-section contains four parts: part A is the precracking area, part B is the unbroken part near the front end of the stop hole, part C is the stop hole, and part D is the crack growth area follows the stop hole, as shown in Figure 17a. Here we define the fatigue life of a specimen as the sum of the crack growth cycles in part B, crack initiation life from the stop hole, i.e., part C, and the crack growth cycles in part D. During the fatigue test, the fatigue machine recorded the total fatigue life of the specimen. Besides, the fatigue life of part B and part D is recorded by the beach marks (see in Figure 17b). Thus, the initiation life of part C can be obtained by subtracting the fatigue life of part B and part D from the overall fatigue life.

Since the crack growth process recorded by the beach marking technique using the variable load ratio of 0.1 and 0.55, where the beach marks only record the crack growth process under the load ratio of 0.1. The cyclic index within the crack growth process under the load ratio of 0.55 is included by the August Wöhler's formula [33], which is

$$C = N(\Delta\sigma)^m, \tag{6}$$

where $\Delta\sigma$ is the stress amplitude of the cyclic load, and N is the cyclic index. Then through Equation (1), the equivalent number of cycles can be calculated as:

$$N_{1e} = N_2(\Delta\sigma_2/\Delta\sigma_1)^m, \tag{7}$$

where N_{1e} is the equivalent number of cycles during the beach marking period, N_2 is the actual number of cycles

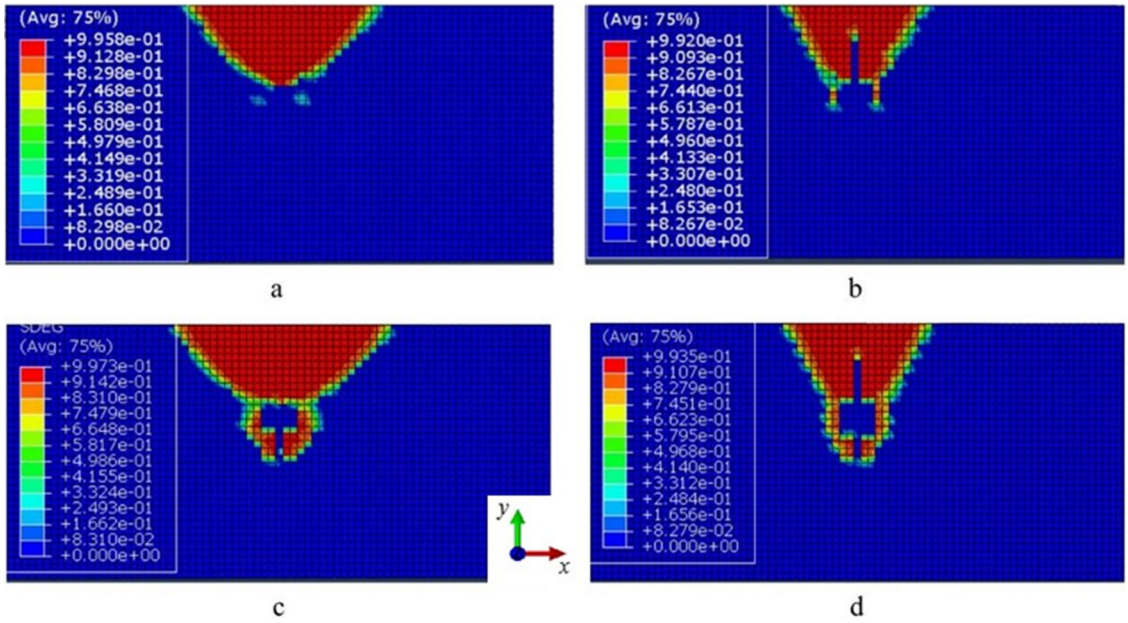

Figure 15. Bond conditions of C28-HS: a) with stop hole, c) with stop hole and crack propagating 10 mm from the stop hole; and C28-HD models: b) with stop hole, d) with stop hole and crack propagating 10 mm from the stop hole.

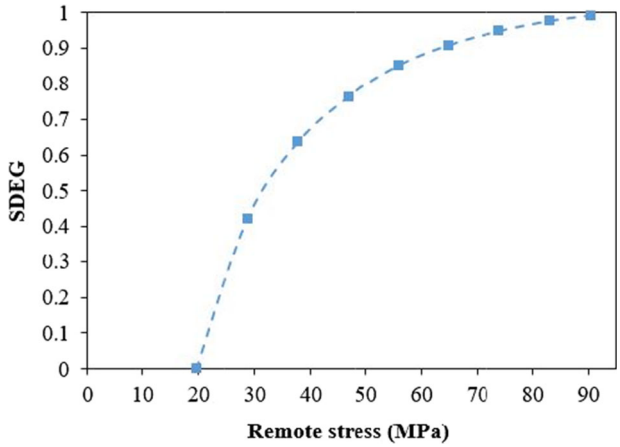

Figure 16. FRP-to-steel interface bond conditions of C28-HS: the SDEG vs. remote stress curve of C28-HS with a 10 mm crack from the stop hole.

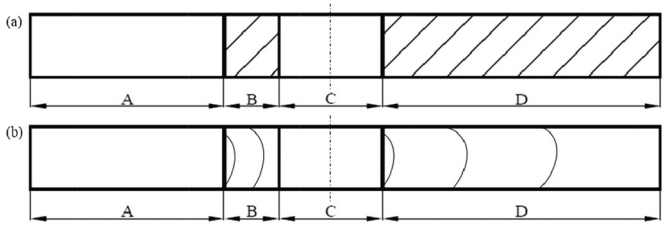

Figure 17. Specimen cross-section: a) different parts divided on the cross-section; b) beach marks recorded on the cross-section.

beach marking period, $\Delta\sigma_1$ is the maximum stress amplitude during the crack propagation process, and $\Delta\sigma_2$ is the stress amplitude of the beach marking load. Thus, the total fatigue life of each specimen was obtained, as listed in Table 7. Note the initiation life is defined as the cyclic numbers till the appearing of the first beach mark from the stop hole. Thus, the initiation life of different specimens in the same group (e.g., C16-HS-1 and C16-HS-2) can be the same.

Figure 18 compares the fatigue life of the specimens using different reinforcement strategies. It indicates that the single-side FRP reinforcement has significantly prolonged the fatigue life of specimens with 16 mm crack length (C16-HS), of averagely 4.81 times more than the specimens that only using the stop hole (C16-H). While when using the FRP to repair the specimens with 22 mm length crack only prolonged the fatigue life of 1.33 times. Although less fatigue life was obtained when using FRP to reinforce even longer crack with 28 mm length, the reinforcement prolonged the fatigue life of averagely 2.90 times. Applying the double-side reinforcement is much more efficient than the single-side reinforcement. The 'C28-HD-1' has dramatically increased the fatigue from averagely from 14,293 cycles to 384,116 cycles, or 25.88 times than the specimens which only repaired by the stop hole. The double-side reinforcement has also prolonged the fatigue life 8.89 times more than the single-side FRP reinforcement.

Figure 19 shows the initiation life, crack propagation life and the ratio of initial life versus crack propagation life, respectively. The single-side FRP reinforcement prolonged the initiation life of 'C16-H-1' of 6.67 times, while the crack propagation life of 3.07 times. Similar results were obtained for specimens with crack length of 22 and 28 mm: 2.09 times and 0.87 times prolongation of initiation and propagation of 'C22-H-1', respectively, and 4.85 times and 2.06 times prolongation of initiation and propagation of 'C28-H-1', respectively. While using double-side FRP reinforcement of 'C28-HD-1' prolonged the initiation life of 'C28-H-1' of 58.67 times, and the crack propagation life of 10.02 times. Figure 19c shows the ratio of the initial life to the total fatigue life, from which it can be found that the FRP reinforcement significantly increases the proportion of the initial life. It indicated that the single-side FRP reinforcement increased the proportion of initiation more than the crack propagation. The double-side FRP reinforcement

Table 7. Experimental results of total fatigue life of each specimen (converted to cyclic numbers under load ratio under 0.1).

Specimen no.	Initiation life (cycles)	Proportion of initiation life (%)	Crack propagation life (cycles)	Proportion of crack propagation life (%)	Total fatigue life (cycles)
C16-H-1	25,629	48.4	27,306	51.6	52,935
C16-H-2	16,543	48.4	17,629	51.6	34,172
C16-HS-1	161,774	63.4	93,461	36.6	255,235
C16-HS-2	161,774	64.4	89,415	35.6	251,189
C22-H-2	16,543	41.1	23,678	58.9	40,221
C22-H-2	8,000	31.2	17,629	68.8	25,629
C22-HS-1	42,172	46.8	47,910	53.2	90,082
C22-HS-2	33,629	53.3	29,430	46.7	63,059
C28-H-1	5,145	31.1	11,398	68.9	16,543
C28-H-2	3,429	28.5	8,613	71.5	12,042
C28-HS-1	25,086	46.0	29,471	54.0	54,557
C28-HS-2	25,086	44.1	31,813	55.9	56,899
C28-HD-1	307,005	71.0	125,625	29.0	432,630
C28-HD-2	238,661	71.1	97,041	28.9	335,702

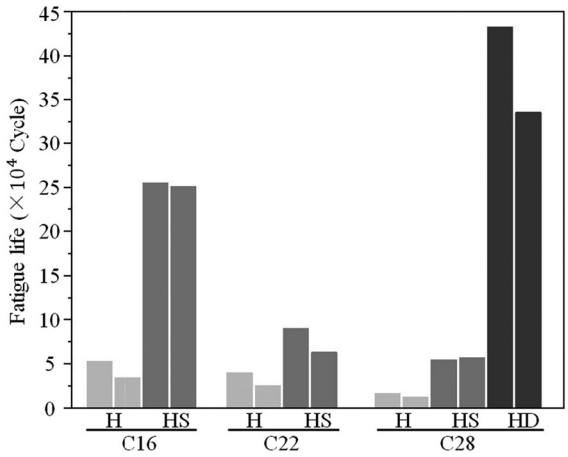

Figure 18. The total fatigue life of each specimen.

increased the initiation life proportion of 71%. That means the fatigue life prolongation mainly owes to the extension of the initiation life. The crack propagation life plays an important role as well.

Here Figures 20 and 21 show the numerical results of the fatigue life, evaluated by the FE model in Section 3.2. Figure 20 indicates the LOGLife data (the logarithm of fatigue life) for the whole double-layer FRP reinforced model, indicating the minimum value locates at the middle area of the stop hole's inner surface, which is $\omega = 3.505$. Based on the fact the bond interface and the composite laminates are not influence by the fatigue loads [34], therefore, the fatigue performance of the FRP-to steel interface and the composite laminates are excluded in this research. Hence, the LOGLife data for these layers should be ignored. Hence, the fatigue life N therefore can be evaluated by

$$N = 10^{\omega}. \tag{8}$$

The crack initiation results of all FE models are listed in Table 8, with a comparison with the experimental results. The maximum error occurs at the C28-H model, which has a very short initiation life, of −18.8%. While the minimum error occurs at the C16-HS, of only −2.4%. In general, the FE results have a good agreement with the experimental results. The experimental results in Figure 18 lack the fatigue life results of C16-HD and C22-HD specimens, the numerical results, therefore, can be used as a supplement to compare the reinforcement effectiveness on different crack lengths.

Together with the numerical results of the crack propagation life evaluated by the FE method, the overall fatigue life of all FE models is shown in Figure 21. The figure clearly illustrates that repairing the cracked specimen at an early stage undoubtedly acquires the longest residual fatigue life. In addition, double-side FRP reinforcement performs significantly more effective than the single-side reinforcement at any stage. Taken the C28 models as an example, the residual fatigue life of the double-side reinforced model is 30 times more than the model only repaired by the stop hole, compared to the single-side reinforced specimens of only 4 times.

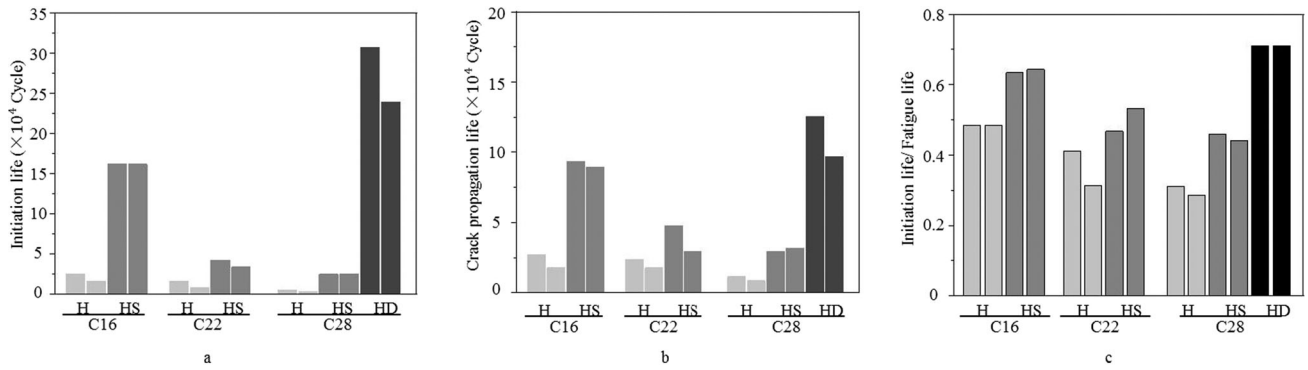

Figure 19. Fatigue life of all specimens: a) initial life; b) crack propagation life; c) the ratio between the initiation life versus total fatigue life.

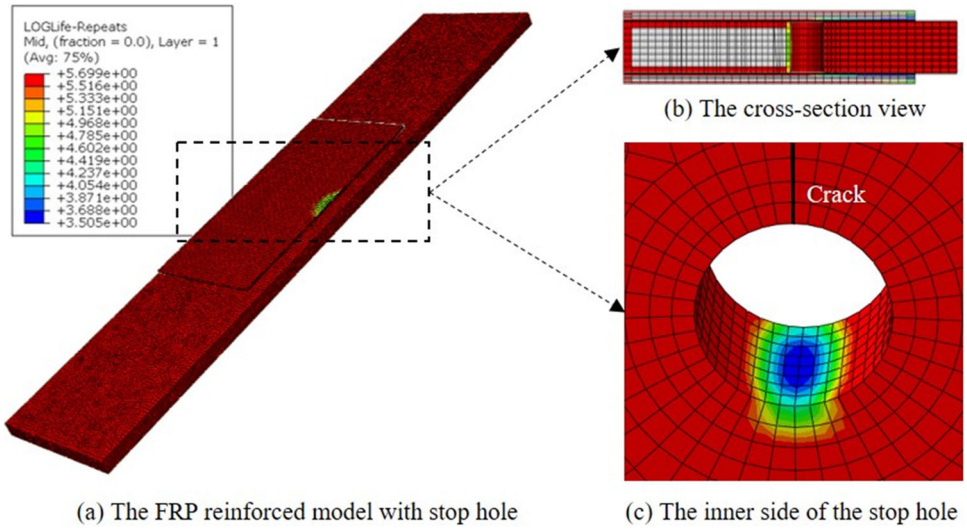

Figure 20. Numerical results of the crack initiation life.

Table 8. The comparison between the experimental results and the numerical results of crack initiation life.

Specimen/model	Test results (*N*)	Numerical results (*N*)	Error
C16-H	21,086	18,614	−11.7%
C16-HS	161,774	157,971	−2.4%
C16-HD	–	522,336	–
C22-H	9,341	8,089	−13.4%
C22-HS	37,900	34,897	−7.9%
C22-HD	–	350,671	–
C28-H	4,287	3,479	−18.8%
C28-HS	25,086	26,658	6.3%
C28-HD	272,833	308,638	13.1%

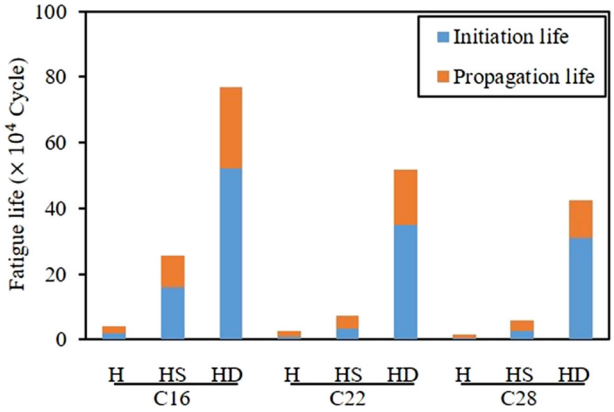

Figure 21. Numerical results of the fatigue life of all FE models.

5. Conclusions

Fatigue crack growth is a serious threat to the structural integrity of metallic structures. Critical cracks need to be repaired instantly in order to avoid more serious failures. In this paper, both the drilling stop hole technique and FRP reinforcement are applied to repair the edge cracked steel plate subjected to cyclic tension. The residual fatigue life, including crack initiation and propagation, have been studied by experimental and numerical approaches. The following conclusions can be drawn:

1) The effect of applying the drilling stop hole technique to prolong residual the fatigue life of the edge cracked steel plate subjected to cyclic tension is limited. While combining the FRP reinforcement method can significantly enhance the repairing effectiveness. In this study, the experimental results shown that combining the double-side FRP reinforcement has prolonged the residual fatigue life of the 28 mm cracked specimen (C28-HD-1) of 25.15 times than the specimen only repaired by the stop hole (C28-H-1): 58.67 times on crack initiation and 10.02 times on the crack propagation.
2) Repairing the cracked plate as early as possible is recommended in order to achieve an optimum repairing effectiveness. The single-side FRP reinforcement performed much less effective on the 28 mm crack than the 16 mm crack. While the double-side FRP reinforcement was still highly effective on longer cracks.
3) Combining the double-side FRP reinforcement with the stop hole performed the best among all reinforcement methods, which have dramatically increased the initiation life from the stop hole and decreased the crack growth rate initiated from the stop hole.
4) The effect of FRP reinforcement is mainly derived from the increasing of the initiation life. In addition, the double-side reinforcement has further promoted this effect. As an example, the initiation life accounts for 71% of the total fatigue life of 'C28-HD' specimens. Its effect on decreasing the crack growth rate performs as the secondary role. This is the reason that the combined methods used in 'C28-HD' performed better than 'C28-D' which uses the double-side FRP reinforcement solely.
5) The single-side FRP reinforcement has changed the initiation position of the fatigue cracks from the stop hole to the opposite side of the reinforcement surface. The reason is the single-side FRP reinforcement has shifted the maximum principle stress value from the middle point to the surface point of the reversed side of the reinforced surface.

Funding

This study was supported by the Fundamental Research Funds for the Central Universities of China [grant number

195218006]. The corresponding author would like to acknowledge China Scholarship Council [grant number 201606950024], and Laboratories for Mechanical Systems Engineering, EMPA-Swiss Federal Laboratories for Materials Science and Technology for funding his research.

ORCID

Zongchen Li http://orcid.org/0000-0003-4784-4684
Xiaoli Jiang http://orcid.org/0000-0001-5165-4942

References

[1] Z. Liu, K. Chen, Z. Li, and X. Jiang, Crack monitoring method for an FRP-strengthened steel structure based on an antenna sensor, Sensors, vol. 17, no. 10, pp. 2394, 2017. DOI: 10.3390/s17102394.

[2] M. Malekan and H. Carvalho, Analysis of a main fatigue crack interaction with multiple micro-cracks/voids in a compact tension specimen repaired by stop-hole technique, J. Strain Anal. Eng. Des., vol. 53, no. 8, pp. 648–662, 2018. DOI: 10.1177/0309324718771124.

[3] Z. Li, X. Jiang, H. Hopman, L. Zhu, Z. Liu, and W. Tang, Experimental investigation on FRP-reinforced surface cracked steel plates subjected to cyclic tension, Mech. Adv. Mater. Struct., pp. 1–15, 2020.

[4] H. Wu, A. Imad, N. Benseddiq, J. T. P. de Castro, and M. A. Meggiolaro, On the prediction of the residual fatigue life of cracked structures repaired by the stop-hole method, Int. J. Fatigue, vol. 32, no. 4, pp. 670–677, 2010. DOI: 10.1016/j.ijfatigue.2009.09.011.

[5] M. Ayatollahi, S. Razavi, and H. Chamani, A numerical study on the effect of symmetric crack flank holes on fatigue life extension of a SENT specimen, Fatigue Fract. Eng. Mater. Struct., vol. 37, no. 10, pp. 1153–1164, 2014. DOI: 10.1111/ffe.12199.

[6] Z.-q. Fu, B.-h. Ji, S.-h. Xie, and T.-j. Liu, Crack stop holes in steel bridge decks: drilling method and effects, J. Cent. South Univ., vol. 24, no. 10, pp. 2372–2381, 2017. DOI: 10.1007/s11771-017-3649-8.

[7] Q.-Q. Yu, X.-L. Zhao, R. Al-Mahaidi, Z.-G. Xiao, T. Chen, and X.-L. Gu, Tests on cracked steel plates with different damage levels strengthened by CFRP laminates, Int. J. Struct. Stab. Dyn., vol. 14, no. 06, pp. 1450018, 2014. DOI: 10.1142/S0219455414500187.

[8] N. Aljabar, X. Zhao, R. Al-Mahaidi, E. Ghafoori, M. Motavalli, and N. Powers, Effect of crack orientation on fatigue behavior of CFRP-strengthened steel plates, Compos. Struct., vol. 152, pp. 295–305, 2016. DOI: 10.1016/j.compstruct.2016.05.033.

[9] E. Ghafoori, A. Schumacher, and M. Motavalli, Fatigue behavior of notched steel beams reinforced with bonded CFRP plates: determination of prestressing level for crack arrest, Eng. Struct., vol. 45, pp. 270–283, 2012. DOI: 10.1016/j.engstruct.2012.06.047.

[10] Q. Yu, T. Chen, X. Gu, and X. Zhao, Boundary element analysis of edge cracked steel plates strengthened by CFRP laminates, Thin-Walled Struct., vol. 100, pp. 147–157, 2016. DOI: 10.1016/j.tws.2015.12.016.

[11] C. Wu, X. L. Zhao, R. Al-Mahaidi, and W. Duan, Effects of CFRP bond locations on the mode I stress intensity factor of centre-cracked tensile steel plates, Fatigue Fract. Eng. Mater. Struct., vol. 36, no. 2, pp. 154–167, 2013. DOI: 10.1111/j.1460-2695.2012.01708.x.

[12] H. Liu, R. Al-Mahaidi, and X.-L. Zhao, Experimental study of fatigue crack growth behaviour in adhesively reinforced steel structures, Compos. Struct., vol. 90, no. 1, pp. 12–20, 2009. DOI: 10.1016/j.compstruct.2009.02.016.

[13] Z. Li, X. Jiang, H. Hopman, L. Zhu, Z. J. T. Liu, and A. F. Mechanics, External surface cracked offshore steel pipes reinforced with composite repair system subjected to cyclic bending: an experimental investigation, vol. 109, pp. 102703, 2020.

[14] J.-H. Choi, and D.-H. Kim, Stress characteristics and fatigue crack behaviour of the longitudinal rib-to-cross beam joints in an orthotropic steel deck, Adv. Struct. Eng., vol. 11, no. 2, pp. 189–198, 2008. DOI: 10.1260/136943308784466224.

[15] S. Reddy, V. Jaswanthsai, M. Madhavan, and V. Kumar, Notch stress intensity factor for center cracked plates with crack stop hole strengthened using CFRP: a numerical study, Thin-Walled Struct., vol. 98, pp. 252–262, 2016. DOI: 10.1016/j.tws.2015.09.018.

[16] F. Alemdar, et al., Use of CFRP overlays to repair fatigue damage in steel plates under tension loading, J. Compos. Constr., vol. 18, no. 4, pp. 04013052, 2014. DOI: 10.1061/(ASCE)CC.1943-5614.0000368.

[17] M. Shahverdi, and S. Mohammadi, Fracture analysis of FRP composites using a meshless finite point collocation method, In: Proceedings of the 4th International Conference on FRP Composites in Civil Engineering, CICE 2008, 2008.

[18] H. Kabir, and M. M. Aghdam, A robust Bézier based solution for nonlinear vibration and post-buckling of random checkerboard graphene nano-platelets reinforced composite beams, Compos. Struct., vol. 212, pp. 184–198, 2019. DOI: 10.1016/j.compstruct.2019.01.041.

[19] K. Zhang, T. Ni, G. Sarego, M. Zaccariotto, Q. Zhu, and U. Galvanetto, Experimental and numerical fracture analysis of the plain and polyvinyl alcohol fiber-reinforced ultra-high-performance concrete structures, Theor. Appl. Fract. Mech., vol. 108, pp. 102566, 2020. DOI: 10.1016/j.tafmec.2020.102566.

[20] GB, Specification for 907A prefilled of military ship (in Chinese), GJB 6055-2007. National Military Standard of P. R. China, 2008.

[21] GB, Test method for properties of resin casting body (in Chinese): GB/T 2567-2008. National Standard of P. R. China, 2008.

[22] ASTM, ASTM E647. Standard Test Method for Measurement of Fatigue Crack Growth Rates, 1994.

[23] E. ASTM, "2899," Standard Test Method for Measurement of Initiation Toughness in Surface Cracks Under Tension and Bending, vol. 3, 2015.

[24] Technical specification for strengthening steel structures (in Chinese), CECS 77:96, 1996.

[25] Z. Li, X. Jiang, H. Hopman, L. Zhu, and Z. Liu, An investigation on the circumferential surface crack growth in steel pipes subjected to fatigue bending, Theor. Appl. Fract. Mech., vol. 105, pp. 102403, 2020. DOI: 10.1016/j.tafmec.2019.102403.

[26] S. Xia and J. Teng, Behaviour of FRP-to-steel bonded joints, Presented at the Proceedings of the International Symposium on Bond Behaviour of FRP in Structures, Hong Kong, 7–9 December 2005, 2005.

[27] O. Basquin, The exponential law of endurance tests, Proc Am. Soc. Test Mater., vol. 10, pp. 625–630, 1910.

[28] C. C. Xinhua Yang, Fatigue and Fracture (2nd Edition), in Chinese. Huazhong University of Science and Technology Press, Wuhan, China, 2019.

[29] Simulia. 2020. FE-SAFE overview. https://www.3ds.com/products-services/simulia/products/fe-safe/

[30] Y. L. Yunrong Luo and Qingyuan Wang, Low cycle fatigue properties of steel structure materials Q235 and Q345 (in Chinese), Adv. Eng. Sci., vol. 44, no. 2, pp. 169–175, 2012.

[31] X. Liu, Y. Zhang, J. Zhu, X. Li, and S. Xue, Fatigue lifetime prediction for oil tube material based on ABAQUS and FE-SAFE, J. Fail. Anal. Prev., vol. 20, no. 3, pp. 936–943, 2020. DOI: 10.1007/s11668-020-00894-x.

[32] P. Paris and F. Erdogan, A critical analysis of crack propagation laws, J. Basic Eng., vol. 85, no. 4, pp. 528–533, 1963. DOI: 10.1115/1.3656900.

[33] A. Wöhler, Über die festigkeitsversuche mit eisen und stahl, Ernst & Korn, 1870.

[34] H. Liu, X. L. Zhao, and R. Al-Mahaidi, The effect of fatigue loading on bond strength of CFRP bonded steel plate joints, Proceedings of the International Symposium on Bond Behaviour of FRP in Structures, pp. 459–464, 2005.